Sensors and Actuators B 252 (2017) 854–861

Contents lists available at ScienceDirect

Sensors and Actuators B: Chemical

journal homepage: www.elsevier.com/locate/snb

# Effect of adding Au nanoparticles and KOH on the electrical and humidity-sensing properties of $WO_3$ particles

Pi-Guey Su*, Wei-Hua Liao

*Department of Chemistry, Chinese Culture University, Taipei 111, Taiwan*

ARTICLE INFO

*Article history:*
Received 26 January 2017
Received in revised form 9 June 2017
Accepted 13 June 2017

*Keywords:*
Humidity sensor
$WO_3$
KOH
Au NPs
Adsorption dynamic analysis
Complex impedance spectra

ABSTRACT

Impedance-type humidity sensors were fabricated from $WO_3$ particles to which had been added KOH or Au nanoparticles (Au NPs). The humidity-sensing (sensitivity and linearity) and electrical properties of the $WO_3$ were improved. Adsorption dynamic analysis and molecular mechanical calculations revealed that the sensitivity of KOH-added $WO_3$ exceeded that of Au NPs-added $WO_3$. The sensor that was made of the KOH-added $WO_3$ exhibited favorable impedance, high sensitivity, good linearity, low hysteresis, a short response/recovery time and high long-term stability over the studied humidity range. Complex impedance spectra were used to investigate the humidity-sensing mechanism of the KOH-added $WO_3$.



## 1. Introduction

Humidity sensors are extensively adopted to improve quality of life and enhance industrial processes. Many materials have been used to fabricate humidity sensors, including polymers [1,2], ceramics [3,4] and composites [5,6]. Ceramic humidity sensors have attracted great interest due to their intrinsic characteristics, such as good reproducibility of the electrical properties, mechanical strength, chemical and physical stability [4]. Among the available materials, metal oxides such as $SnO_2$, $TiO_2$, ZnO, $Fe_2O_3$, $Al_2O_3$, $In_2O_3$ and $WO_3$, are the most popular sensing materials for humidity sensors [4]. $WO_3$ has been considered as a promising sensing material for detecting humidity due to its simple design, low cost, long term stability, high reliability and fast response [4,7]. Adding Ag [8], $SnO_2$ [9], $TiO_2$ [10–13] or $Cr_2O_3$ [14] is an effective means of improving the performance of $WO_3$-based humidity sensors.

Alkali ions, such as $Li^+$ or $K^+$ are used to increase the sensitivity of $Fe_2O_3$- [15], $SnO_2$- [16], $TiO_2$- [17,18] and ZnO-based [19,20] semiconductor humidity sensors because they are associated with a large number of chemisorption sites for water vapor owing to their small sizes and the high local charges. Noble nanometals such as Pt, Pd and Au have also been used as effective additives for chemical sensor applications [21,22]. To the best of our knowledge, not any humidity sensor that is based on $WO_3$ with added KOH or Au nanoparticles (Au NPs) has yet been fabricated. Moreover, the effect of adding Au NPs or KOH on humidity-sensing properties of the $WO_3$ has not been studied. In this work, impedance-type humidity sensors that are based on $WO_3$, and whose conductivity and sensitivity were modified by adding KOH or Au NPs, were fabricated and characterized. The electrical properties of KOH-added $WO_3$ and Au NPs-added $WO_3$ were studied as functions of RH, with special emphasis on sensitivity and linearity. The dynamics of the adsorption of water vapor molecules onto KOH-added and Au NPs-added $WO_3$ that were coated on an electrode of quartz crystal microbalance (QCM) was also considered to elucidate the sensitivity of the $WO_3$-based sensing materials herein. The microstructural characteristics of the $WO_3$ were investigated by scanning electron microscopy (SEM) and atomic force microscopy (AFM). Complex impedance spectra were obtained to elucidate the involvement of ions in conduction by KOH-added $WO_3$. The humidity-sensing characteristics of the $WO_3$-based sensing materials, including their sensitivity, hysteresis, response time, recovery time and long-term stability, were also studied.

* Corresponding author.
*E-mail addresses:* spg@faculty.pccu.edu.tw, spg@ulive.pccu.edu.tw (P.-G. Su).

http://dx.doi.org/10.1016/j.snb.2017.06.094
0925-4005/

## 2. Experimental

### 2.1. Materials and preparation of impedance- type humidity sensor

In the preparation of ball-milled $WO_3$ powders, 10 g of $H_2WO_4$ powder (Aldrich, 99%) was ball-milled in ethanol solution for 24 h. The slurry thus formed was dried at 110 °C and calcined at 600 °C for 4 h in an air stream to form ball-milled $WO_3$ powders. The natural $WO_3$ powders were prepared by directly calcining $H_2WO_4$ powder at 600 °C for 4 h in air.

Au NPs were prepared using the method in the literature [23]. The Au NPs colloidal particles were prepared by adding 38.8 mM sodium citrate (Shimakyu's Pure. Chemicals, 99%) to boiling aqueous 1 mM $HAuCl_4$ (Alfa Aesar, 99%). The solution was boiled for 15 min with vigorous stirring, and then allowed to cool to room temperature.

Natural $WO_3$ precursor slurry solution was prepared by adding 2 g of natural $WO_3$ powders to 5 mL deionized water (DIW) with vigorous stirring. The preparation of ball-milled $WO_3$ precursor slurry solution were the same that of the natural $WO_3$ precursor slurry solution. KOH-added $WO_3$ and Au NPs-added $WO_3$ precursor slurry solutions were prepared by dispersing the 2 g of as-prepared ball-milled $WO_3$ powders in 5 mL of KOH (Wako Pure Chemical Industries, Ltd) solution or as-prepared Au NPs colloidal particles, then and the above as-prepared mixing slurry solution was stirred for 12 h. The amounts of added KOH were varied 0.01, 0.05, 0.1 and 0.2 mol/L. The amounts of added Au NPs were 0.1 mol/L.

Fig. 1(a) schematically depicts the microstructure of the impedance-type humidity sensor. The interdigitated gold electrodes were made on an alumina substrate by screen-printing, and then calcined at 850 °C for 1 h in air. Then, 20 μL of the as-prepared natural $WO_3$, ball-milled $WO_3$, KOH-added $WO_3$ and Au NPs-added $WO_3$ precursor slurry solutions were drop-coated onto alumina, which was then thermally treated at 60 °C for 0.5 h in air. The thicknesses of the natural $WO_3$, ball-milled $WO_3$, KOH-added $WO_3$ and Au NPs-added $WO_3$ were about 27.2 (±0.6), 26.3 (±0.5), 26.5 (±0.5) and 26.8 (±0.4) μm, respectively.

### 2.2. Instruments and analysis

The surface microstructure of the natural $WO_3$, ball-milled $WO_3$, KOH-added $WO_3$ and Au NPs-added $WO_3$ that were coated on an alumina substrate was investigated using a scanning electron microscope (SEM), a field emission scanning electron microscope (FE-SEM, FEI company, Nova NanoSEM™ 230) and atomic force microscopy (AFM, Ben-Yuan, CSPM 4000). Energy dispersive spectrometer (EDS) was used to analyze the element of the $WO_3$-based materials.

Fig. 1(b) presents the humidity-sensing measurement system. A divided flow humidity generator was used as the principal facility for producing the testing humidity, as same as previously reported [24]. The required humidity was produced by adjusting the ratio of dry and to humid air that were generated by the divided-flow humidity generator at a total flow rate of 10 L/min. The flow rates were regulated with mass flow meters and controllers (Hastings). The required humidity (RH values) was adjusted according to readings from a humidity hygrometer (accuracy of ±0.1% RH, Rotronic) that was calibrated at the CMS/NML (Center for Measurement Standards/National Measurement Laboratory) humidity laboratory. The impedance of the sensor thus formed was measured as a function of RH using an LCR meter (Inductance (L), Capacitance (C) and Resistance (R)) in a temperature-controlled chamber (Thermo-HAAKE) under the conditions of a measurement frequency of 1 kHz, an applied voltage of 1 V, an ambient temperature of 25 °C, shown in Fig. 1(b Path I).

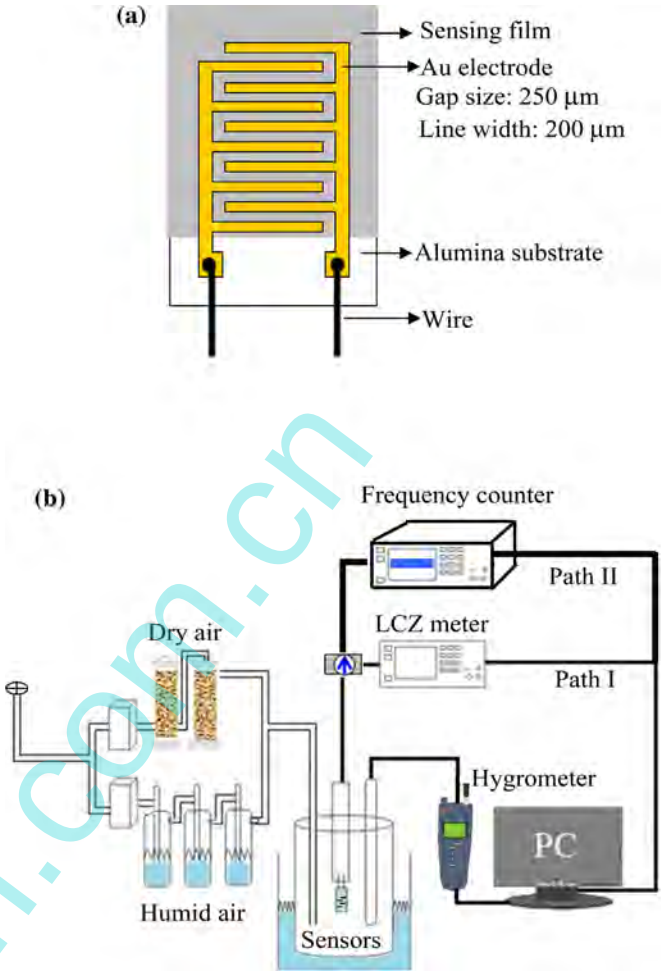


**Fig. 1.** (a) Structure of humidity sensor. (b) Schematic structure of the impedance (Path I) and QCM (Path II) measurement of sensors and the humidity atmosphere controller.

The dynamics of the adsorption of water vapor molecules onto ball-milled $WO_3$, KOH-added $WO_3$ and Au NPs-added $WO_3$ was investigated by quartz crystal microbalance (QCM) technique. The AT-cut quartz crystals with a fundamental resonance frequency of 10 MHz and a frequency counter were obtained from ANT Technologies Corp., Taiwan. The surface area of the gold electrode on a QCM was 0.102 $cm^2$. Both sides of the QCM electrode were coated with the as prepared KOH-added $WO_3$ and Au NPs-added $WO_3$ precursor slurry solutions by spin coating at a rate of 2000 rpm for 120 s, followed by heating at 60 °C for 15 min in air. Each QCM sensor was connected to a suitable holder and placed in the divided flow humidity generator measuring chamber and was connected to an oscillator. The frequency shift of QCM sensors due to the humidity adsorption was measured using the frequency counter, and then the output signal was transferred to a computer, shown in Fig. 1(b, Path II). Sauerbrey [25] first derived the quantitative relationship between changes in frequency $\Delta f$ (Hz) of the piezoelectric crystal and mass change caused by mass loading on the piezoelectric crystal surface as follows:

$$\Delta f = (-2.3 \times 10^{-6} \frac{f_o^2}{A}) \Delta m \quad (1)$$

where $f_o$ (MHz) denotes the basic frequency of the unloaded piezoelectric crystal, $A$ ($cm^2$) represents the surface area of the electrode, and $\Delta m$ (g) is the change in mass on the crystal surface.

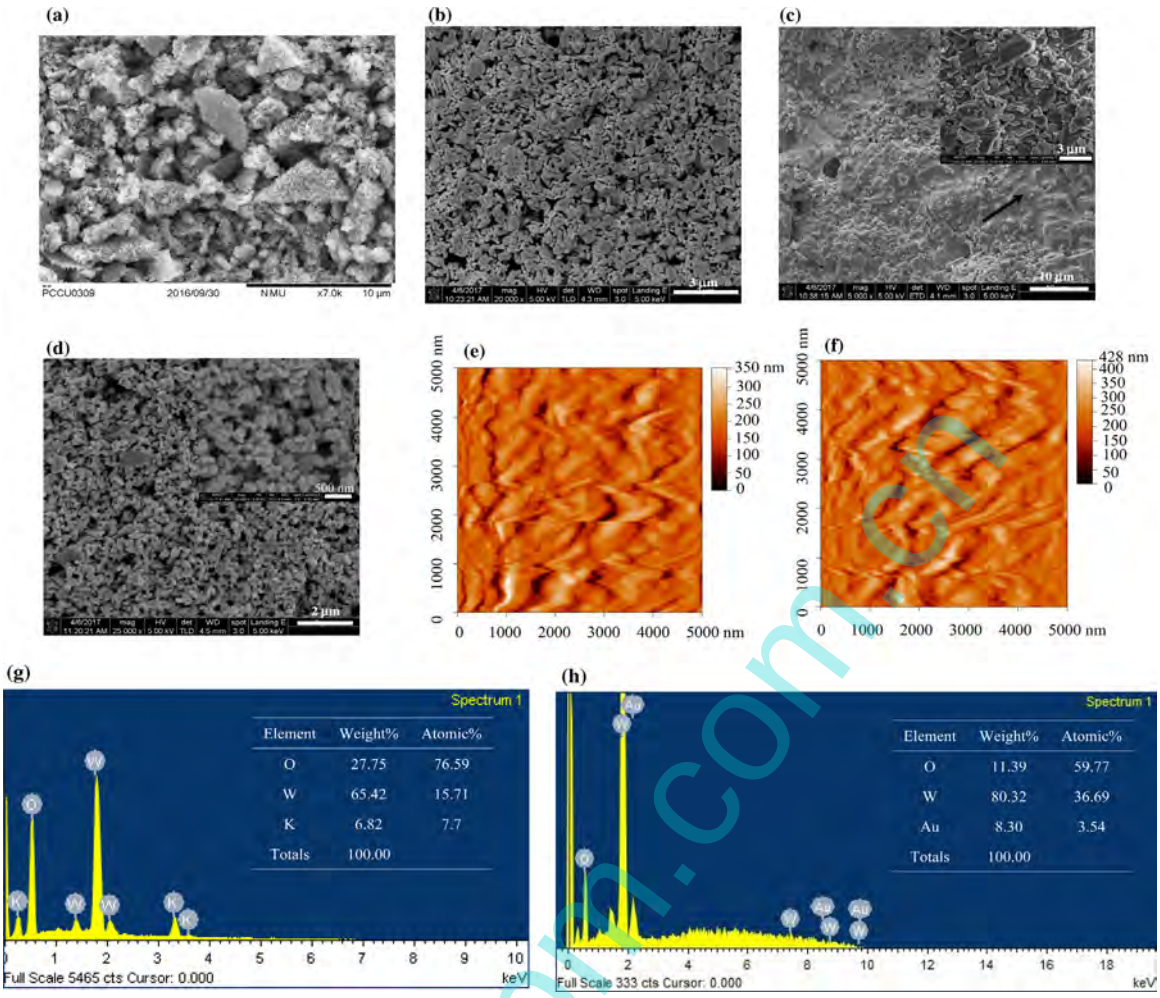


**Fig. 2.** SEM images of (a) Natural $WO_3$, (b) Ball-milled $WO_3$, (c) KOH-added $WO_3$ and (d) Au NPs-added $WO_3$. AFM images of (e) KOH-added $WO_3$ and (f) Au NPs-added $WO_3$. EDS spectra of (g) KOH-added $WO_3$ and (h) Au NPs-added $WO_3$.

## 3. Results and discussion

### 3.1. Surface microstructure of natural $WO_3$, ball-milled $WO_3$, KOH-added $WO_3$ and Au NPs-added $WO_3$

Fig. 2(a)–(d) show SEM images of natural $WO_3$, ball-milled $WO_3$, KOH-added $WO_3$ and Au NPs-added $WO_3$, respectively. The surface of these films had a rough porous structure. The sizes of the natural $WO_3$, ball-milled $WO_3$, KOH-added $WO_3$ and Au NPs-added $WO_3$ were about 4.57 μM, 417 nm, 574 nm and 310 nm, respectively. Compared with Fig. 2(b), Fig. 2(c) shows a thin film covered the $WO_3$ particles when KOH was added to it (as indicated by the arrow). The high-magnification SEM image (inset in Fig. 2(c)) reveals that obviously aggregation of the $WO_3$ was observed due to the added KOH. No obvious aggregation of $WO_3$ was observed when Au NPs was added to it (Fig. 2(d)). Moreover, the high-magnification SEM image (inset in Fig. 2(d)) shows that the Au NPs coated the $WO_3$ was not clear. Fig. 2(e) and (f) show the surface topography of 5 μm × 5 μm KOH-added $WO_3$ and Au NPs-added $WO_3$. The root mean square (RMS) roughness values of the KOH-added $WO_3$ and Au NPs-added $WO_3$ were 41.6 and 47.3 nm, respectively. The values of roughness of KOH-added $WO_3$ and Au NPs-added $WO_3$ did not differ significantly from each other. The EDS analysis demonstrated that the KOH (Fig. 2(g)) and Au NPs (Fig. 2(h)) were surely added to the $WO_3$.

**Table 1**
Sensitivity and linearity of humidity sensors that were made of natural $WO_3$, ball-milled $WO_3$, KOH-added $WO_3$ and Au NPs-added $WO_3$.

| | Sensing curve | |
|---|---|---|
| | Sensitivity[a] (log Z/%RH) | Linearity[b] ($R^2$) |
| Natural $WO_3$ | −0.0202 | 0.9628 |
| Ball-milled $WO_3$ | −0.0388 | 0.9684 |
| Au NPs-added $WO_3$ | −0.0392 | 0.9754 |
| 0.01 M KOH-added $WO_3$ | −0.0297 | 0.9884 |
| 0.05 M KOH-added $WO_3$ | −0.0291 | 0.9872 |
| 0.1 M KOH-added $WO_3$ | −0.0484 | 0.9646 |
| 0.2 M KOH-added $WO_3$ | – | – |

[a] Sensitivity was defined as the slope of the logarithmic impedance versus relative humidity plot in the range 10–90% RH.
[b] Linearity was shown as the correlation coefficient of the logarithmic impedance versus relative humidity plot in the range 10–90% RH.

### 3.2. Effect of adding Au NPs and KOH on electrical and humidity-sensing properties of $WO_3$

Fig. 3(a) plots the impedances of the natural $WO_3$, ball-milled $WO_3$, KOH-added $WO_3$ and Au NPs-added $WO_3$ as functions of relative humidity. The measurements were made at 25 °C, an AC voltage of 1 V, and a frequency of 1 kHz. Table 1 presents results concerning sensitivity and linearity based on the fitted line from 10 to 90% RH, where sensitivity is defined as the slope of the logarithmic impedance (log Z) versus%RH and linearity, which is a

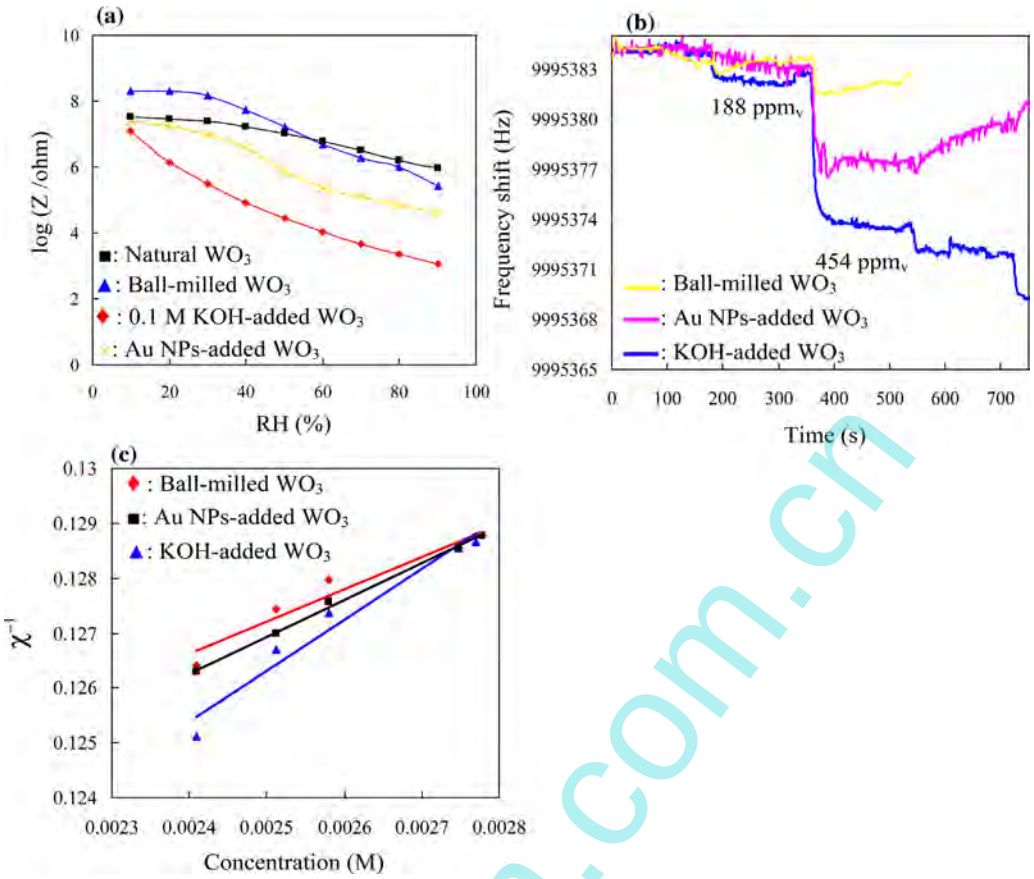


**Fig. 3.** (a) Impedance versus relative humidity plots for humidity sensors. (b) Frequency shifts (Hz) as a function of time (s) for different volume ratio of the moist air on KOH-added $WO_3$ and Au NPs-added $WO_3$. (c) Linear plot of the reciprocal of relaxation time ($\chi^{-1}$) against vapor concentration (M) for KOH-added $WO_3$ and Au NPs-added $WO_3$.

correlation coefficient that is defined as the R-squared value of the fitted line. The sensitivity of the sensors declined in the order KOH-added $WO_3$ > Au NPs-added $WO_3$ > ball-milled $WO_3$ > natural $WO_3$. The sensitivity of ball-milled $WO_3$ exceeded that of natural $WO_3$ was related to the fact that the size of $WO_3$ powders decreased from 4.57 μM to 417 nm, presenting more surface active sites for adsorbing water molecules, and thereby improved the sensitivity of ball-milled $WO_3$. The ball-milled $WO_3$ had higher impedance than that of natural $WO_3$ at low humidity (<60% RH) because smaller grains had more grain contacts. The ball-milled $WO_3$ exhibited no obvious variation in impedance in the range 10–30% RH because its impedance was so high (about 200 MΩ). Adding KOH or Au NPs to ball-milled $WO_3$ effectively reduced this high impedance and improved the sensitivity. Moreover, the sensitivity of the KOH-added $WO_3$ exceeded that of Au NPs-added $WO_3$. The sensitivity of the 0.1 M KOH-added $WO_3$ exceeded that of $WO_3$ (alone), because KOH is a strong electrolyte, and generating a high local charge density and a strong electrostatic field on $WO_3$ indicating that water molecules are more easily adsorbed on 0.1 M KOH-added $WO_3$ than on $WO_3$ alone.

The dynamics of adsorption of water molecules onto the ball-milled $WO_3$, KOH-added $WO_3$ and Au NPs-added $WO_3$, measured using the by QCM technique, revealed that the sensitivity of the KOH-added $WO_3$ exceeded that of ball-milled $WO_3$ and Au NPs-added $WO_3$. Fig. 3(b) plots the dynamic frequency shifts of ball-milled $WO_3$, KOH-added $WO_3$ and Au NPs-added $WO_3$ versus time for volume concentrations of moisture in air in the range of 188–454 $ppm_v$ (6.2–16.2% RH). The dynamic frequency shift of KOH-added $WO_3$ exceeded that of ball-milled $WO_3$ and Au NPs-added $WO_3$. Therefore, water molecules were more easily adsorbed onto the KOH-added $WO_3$ than onto the Au ball-milled $WO_3$ and NPs-added $WO_3$. To compare the adsorption behaviors of water molecules on ball-milled $WO_3$, KOH-added $WO_3$ and Au NPs-added $WO_3$, the binding rate constant is calculated as described by Okada et al. [26] and Okahata et al. [27]. Eq. (2) describes the binding between a sensing film and molecules of water vapor.

$$\text{Sensing films} + \text{water vapor molecules} \quad \text{Sensing films} - \text{water vapor molecules} \tag{2}$$

where $k_1$ and $k_{-1}$ are the adsorption and desorption rate constants, respectively. The formed amount of water vapor molecules, $\Delta m_t$, on the ball-milled $WO_3$, KOH-added $WO_3$ and Au NPs-added $WO_3$ sensing layers at time t, was calculated by Eqs. (3)–(6) under Langmuir isotherm adsorption conditions [26,27]:

$$[\text{adsorbed vapor molecules}]_t = [\text{adsorbed vapor molecules}]_\infty [1 - \exp(\frac{-t}{\chi})] \tag{3}$$

$$\Delta m_t = \Delta m_\infty [1 - \exp(\frac{-t}{\chi})] \tag{4}$$

$$\frac{-t}{\chi} = \ln[\frac{(\Delta m_\infty - \Delta m_t)}{\Delta m_\infty}] \tag{5}$$

$$\chi^{-1} = k_1\,[\text{adsorbed vapor molecules}] + k_{-1} \tag{6}$$

where $\Delta m_\infty$ is the maximal amount of water vapor molecules that are adsorbed on the sensing films at $t \to \infty$ and $\chi$ is the relaxation time. Fig. 3(c) plots the linear correlation between the reciprocal of relaxation time ($\chi^{-1}$) of adsorption and the concentration of

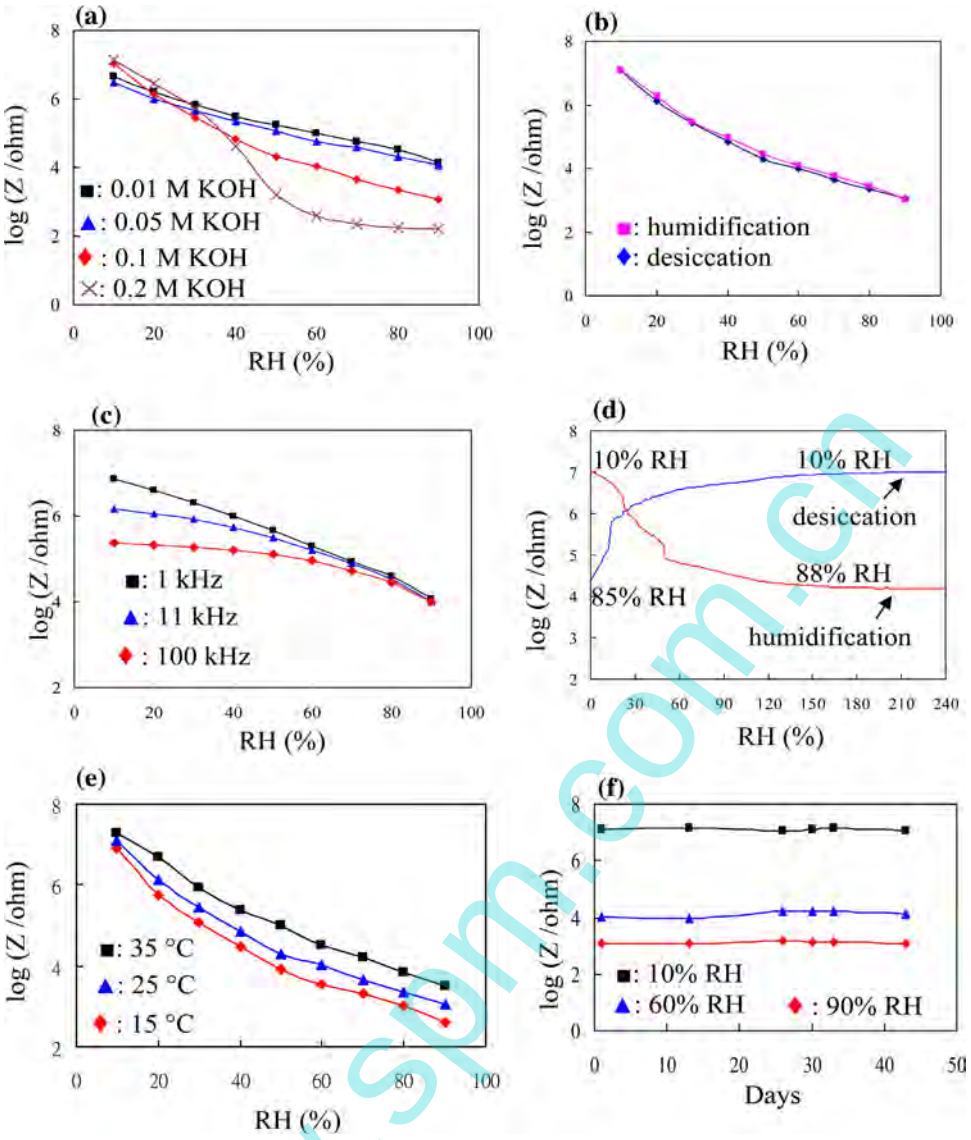


**Fig. 4.** (a) Ball-milled $WO_3$ added various dosages of KOH, (b) Hysteresis of the humidity sensor, (c) Effect of applied frequency on the response of the humidity sensor, (d) Response-recovery properties of the humidity sensor, (e) Effect of temperature on the response of the humidity sensor, (f) long-term stability of the humidity sensor.

**Table 2**
Kinetic parameters for adsorption and desorption of water vapor molecules onto ball-milled $WO_3$, KOH-added $WO_3$ and Au NPs-added $WO_3$.

| Thin films | Adsorption rate constant, $k_1$ ($M^{-1}\,s^{-1}$) | Desorption rate constant, $k_{-1}$ ($s^{-1}$) | Association constant, $K$ ($M^{-1}$) |
|---|---|---|---|
| Ball-milled $WO_3$ | 5.9002 | 0.1125 | 52.44 |
| Au NPs-added $WO_3$ | 6.1816 | 0.1102 | 60.63 |
| KOH-added $WO_3$ | 9.3202 | 0.1030 | 90.49 |

water vapor on the ball-milled $WO_3$, KOH-added $WO_3$ or Au NPs-added $WO_3$ (Eq. (6)). The values of $k_1$ and $k_{-1}$ were obtained from the slope and intercept of the curves in Fig. 3(c). Table 2 presents $k_1$, $k_{-1}$ and the association constant $K$ ($=\frac{k_1}{k_{-1}}$) for water vapor on the sensing films. The adsorption rate constant ($k_1$) followed the order KOH-added $WO_3$ > Au NPs-added $WO_3$ > ball-milled $WO_3$. This experimental result reveals that water molecules are adsorbed more easily on KOH-added $WO_3$ than on ball-milled $WO_3$ and Au NPs-added $WO_3$. The KOH-added $WO_3$ had a larger association constant $K$ (90.49 $M^{-1}$) than Au NPs-added $WO_3$ (60.63 $M^{-1}$) and ball-milled $WO_3$ (52.44 $M^{-1}$), so water molecules were adsorbed more easily and strongly on KOH-added $WO_3$ than on ball-milled $WO_3$ and Au NPs-added $WO_3$. These results reveal that the KOH-added $WO_3$ was more sensitive to water molecules than was the ball-milled $WO_3$ and Au NPs-added $WO_3$. Therefore, the humidity sensor that was made of KOH-added $WO_3$ was further tested to elucidate its humidity-sensing properties and mechanism.

### 3.3. Humidity-sensing properties of KOH-added $WO_3$

Fig. 4(a) plots the effect of the amount of added KOH on the impedance and humidity-sensing properties of KOH-added $WO_3$, as functions of relative humidity. At low humidity (<20% RH), as the amount of added KOH increased up to 0.1 M, the impedance decreased. When the amount of added KOH was 0.2 M, the impedance was almost independent of RH in the range 60–90% RH. This finding may be explained by the fact that KOH has a very

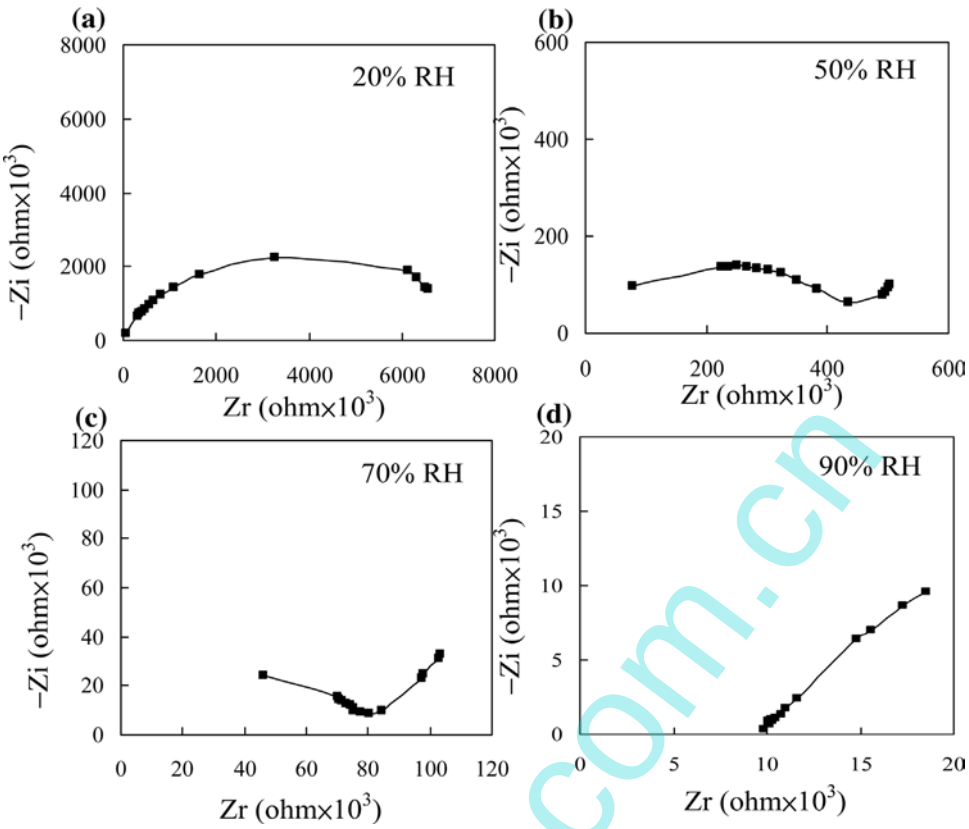


**Fig. 5.** Complex impedance plots of KOH-added $WO_3$ at (a) 20% RH, (b) 50% RH, (c) 70% RH and (d) 90% RH.

**Table 3**
Humidity sensor performance of this work compared with the literatures.

| Sensor type | Sensing material | Working range (%RH) | Sensitivity | Hysteresis (%RH) | Response/recovery time (s) | References |
|---|---|---|---|---|---|---|
| Impedance-type | KOH-added $WO_3$ | 10–90 | 0.0484[a] $10^4$ [b] | <1.5 | 46/52 | This work |
| Resistance-type | $WO_3$-$SnO_2$ nanocomposite | 10–90 | 2.78[c] | 5.4 | 121/453 | [9] |
| Impedance-type | KCl-doped $SnO_2$ nanofibers | 11–95 | $10^5$ [b] | 3 | 5/6 | [16] |
| Impedance-type | KCl-doped $TiO_2$ nanofibers | 11–95 | $10^4$ [b] | – | 3/3 | [17] |
| Impedance-type | LiCl-doped ZnO nanofibers | 11–95 | $10^4$ [b] | 2 | 3/6 | [20] |
| Impedance-type | $TiO_2$ NPs/polypyrrole | 30–90 | 0.0306 | <3 | 40 | [31] |
| Impedance-type | PAMPS[d]/NaCl/$K_2CO_3$ | 20–90 | 0.0260 | <8 | 60 | [32] |
| Capacitance-type | $MgTiO_3$/LiF | 15–80 | 3.28[e] | 3 | 70/5 | [33] |
| Capacitance-type | ZnO cauliflowers | 11.3–94.6 | 17.04[f] | 4.16 | 20/3 | [34] |

[a] The sensitivity was calculated as the slope (log Z/%RH)of the sensing curve in the working range.
[b] The sensitivity was calculated as the impedance variations of the sensor changed during the working range.
[c] The sensitivity was calculated by ΔR/ΔRH (MΩ/%RH) during the working range.
[d] PAMPS: poly(2-acrylamido-2-methylpropane sulfonate).
[e] The sensitivity was calculated by ΔC/ΔRH (pF/%RH) during the working range.
[f] The sensitivity was calculated by ΔC/ΔRH (nF/%RH) during the working range.

high dissociation constant ($6.63 \times 10^{10}$) [28,29], and so is easily and completely dissociated in a highly humid atmosphere. The sensitivity increased from 0.0297 to 0.0484 with the addition of KOH. Since it had both the highest sensitivity and the highest sensing linearity, the 0.1 M KOH-added $WO_3$ was further tested to evaluate its humidity-sensing characteristics and humidity-sensing mechanism.

Fig. 4(b) shows the hysteresis property of the humidity sensor. The hysteresis (between humidification and desiccation, measured over an RH range of 10–90%) was less than 1.5% RH. Fig. 4(c) shows the effect of the applied frequency on the response of the humidity sensor, the impedance was measured at frequencies of 1, 11 and 100 kHz at a voltage of 1 V. The curve of impedance versus RH was most linear at 1 kHz. The impedance of the humidity sensor clearly decreased as the frequency increased at low RH because the adsorbed water could not be polarized (at RH < 60%) at a very high frequency [30]. Fig. 4(d) plots the response and recovery of the humidity sensor that was measured of which measurements were made at 25 °C and 1 kHz. The response time ($T_{res.95\%}$) is defined as the time taken for the impedance of the humidity sensor to response 95% of the maximum change after humidification from 10 to 88% RH. The recovery time ($T_{rec.95\%}$) is defined at the time required for the humidity sensor to recover 95% of the maximum change in impedance after desiccation from 85 to 10% RH. The response time ($T_{res.95\%}$) and recovery ($T_{rec.95\%}$) time of the sensor were 46 and 52 s, respectively. The response time included the equilibration time of the water vapor inside the testing chamber so the actual response time of the sensor was much shorter than that recorded. Three batches of five humidity sensors each were fabricated to analyze their reproducibility. For the three batches of sensors, the reproducibility, given by a coefficient of variation, was in the range 0.45–1.52 at an RH of between 10 and 90%. Fig. 4(e)

plots the log-impedance of the humidity sensor versus temperature. As the temperature increased, the RH characteristic curve shifted to lower impedance. The mean temperature coefficient at 15–35 °C was within −1.1% RH/°C over the humidity range 10 ~ 90% RH. Fig. 4(f) plots the long-term stability. The humidity sensor impedance did not significantly vary for at least 43 days at the tested RH values of 10, 60, and 90% RH.

Table 3 compares the humidity sensing properties of the presented humidity sensor with those in the literature [9,16,17,20,31–34]. The developed humidity sensor that was made of $WO_3$ to which was added KOH exhibited good hysteresis, and a comparable sensitivity to, those of the impedance-/resistance-type sensors that were made of $WO_3$-$SnO_2$ nanocomposite material [9], KCl-doped $SnO_2$ nanofibers [16], KCl-doped $TiO_2$ nanofibers [17] and LiCl-doped ZnO nanofibers [20]. Moreover, the presented humidity sensor had higher sensitivity and lower hysteresis than the sensor that was made with polymers-based (poly(2-acrylamido-2-methylpropane sulfonate and polypyrrole)) [31,32]. However, the capacitance-type sensors that were made of $MgTiO_3$/LiF [33] and ZnO cauliflowers [34] had higher sensitivity and shorter response/recover time than that of the presented humidity sensor.

### 3.4. Complex impedance

Impedance spectroscopy is a powerful method to investigate the conduction mechanisms of humidity sensors. Therefore, the conduction mechanism of the KOH-added $WO_3$ was studied using the obtained complex impedance plots. Fig. 5(a)–(d) show the complex impedance spectra of the KOH-added $WO_3$ at various humidities. The impedance measurements were carried out in the frequency range from 60 Hz to 100 kHz at humidities from 20 to 90% RH, an ac voltage of 1 V and 25 °C. In the impedance spectra, $Z_r$ is the real part of the impedance Z, and is plotted on the real axis, and $Z_i$ is the imaginary part of Z, and is plotted on the imaginary axis. A semicircular plot of film impedance was obtained at 20% RH (Fig. 5(a)), which was mainly resulted from the intrinsic impedance of the material [5,35]. As RH increased to 50–70% RH, a line on the complex plot appeared at low frequencies and its length increased with RH (Fig. 5(b) and (c)). The plot of impedance became a straight line at 90% RH (Fig. 5(d)). The straight line at low frequencies represents was mainly considered to be the contribution of ions ($K^+$ and $H_3O^+$) [5,35–37]. Therefore, from the view of the complex impedance plots, the ions ($K^+$ and $H_3O^+$) dominated the variation of conductance of the sensor with%RH.

## 4. Conclusions

The sensitivity and linearity of ball-milled $WO_3$ exceeded that of natural $WO_3$ because of decreasing the size of $WO_3$ powders. Adding KOH and Au NPs to ball-milled $WO_3$ greatly improved its conductance and sensitivity. An adsorption dynamic analysis and molecular mechanical calculations revealed that the association constant *K* for water molecules on KOH-added $WO_3$ exceeded that for ball-milled $WO_3$ and Au NPs-added $WO_3$, so the sensitivity of KOH-added $WO_3$ exceeded that of ball-milled $WO_3$ and Au NPs-added $WO_3$. The humidity sensor that was made of 0.1 M KOH-added $WO_3$ had the highest sensitivity (slope = −0.0484) and good linearity ($R^2$ = 0.9646) between the logarithmic impedance (log Z) and RH from 10 to 90%, negligible hysteresis (less than 1.5% RH), a short response time (46 s), a short recovery time (52 s), and good long-term stability (at least 43 days), as measured at 1 V, 1 kHz and 25 °C. The plots of the complex impedance of the KOH-added $WO_3$ with in different RH revealed that the curves changed from semicircular to linear as RH increased, revealing $K^+$ and $H_3O^+$ ions dominated the humidity-sensing mechanism of the KOH-added $WO_3$.

## Acknowledgement

The authors thank the Ministry of Science and Technology (grant no. MOST 105-2113-M-034-001) of Taiwan for support.

## References

[1] Y. Sakai, Y. Sadaoka, M. Matsuguchi, Humidity sensors based on polymer thin films, Sens. Actuators B 35-36 (1996) 85–90.
[2] B. Adhikari, S. Majumdar, Polymers in sensor applications, Prog. Polym. Sci. 29 (2004) 699–766.
[3] G. Sberveglieri, R. Murri, N. Pinto, Characterization of porous $A1_2O_3$-$SiO_2$/Si sensor for low and medium humidity ranges, Sens. Actuators B 23 (1995) 177–180.
[4] T.A. Blank, L.P. Eksperiandova, K.N. Belikov, Recent trends of ceramic humidity sensors development: a review, Sens. Actuators B 228 (2016) 416–442.
[5] C.D. Feng, S.L. Sun, H. Wang, C.U. Segre, J.R. Stetter, Humidity sensing properties of nation and sol-gel derived $SiO_2$/nation composite thin films, Sens. Actuators B 40 (1997) 217–222.
[6] Y. Li, M.J. Yang, Y. She, Humidity sensors using in situ synthesized sodium polystyrenesulfonate/ZnO nanocomposites, Talanta 62 (2004) 707–712.
[7] A.S. Garde, Humidity sensing properties of $WO_3$ thick film resistor prepared by screen printing technique, J. Alloys Compd. 617 (2014) 367–373.
[8] N.K. Pandey, K. Tiwari, A. Roy, Ag doped $WO_3$ nanomaterials as relative humidity sensor, IEEE Sens. J. 11 (2011) 2911–2918.
[9] A. Roy, N.K. Pandey, V. Shakya, A. Kumar, Humidity sensor based on synthesized $WO_3$–$SnO_2$ nanocomposites, Energy Environ. Focus 2 (2013) 126–132.
[10] K.O. Rocha, S.M. Zanetti, Structural and properties of nanocrystalline $WO_3$/$TiO_2$-based humidity sensors elements prepared by high energy activation, Sens. Actuators B 157 (2011) 654–661.
[11] S.M. Zanetti, K.O. Rocha, J.A.J. Rodrigues, E. Longo, Soft-chemical synthesis, characterization and humidity sensing behavior of $WO_3$/$TiO_2$ nanopowders, Sens. Actuators B 190 (2014) 40–47.
[12] P.M. Faia, E.L. Jesus, C.S. Louro, $TiO_2$:$WO_3$ composite humidity sensors doped with ZnO and CuO investigated by impedance spectroscopy, Sens. Actuators B 203 (2014) 340–348.
[13] P.M. Faia, J. Libardi, C.S. Louro, Effect of $V_2O_5$ doping on p- to n-conduction type transition of $TiO_2$:$WO_3$ composite humidity sensors, Sens. Actuators B 222 (2016) 952–964.
[14] S. Pokhrel, K.S. Nagaraja, Electrical and humidity sensing properties of chromium(III) oxide–tungsten(VI) oxide composites, Sens. Actuators B 92 (2003) 144–150.
[15] G. Neri, A. Bonavita, S. Galvagno, C. Pace, S. Patané, A. Arena, Humidity sensing properties of Li-iron oxide based thin films, Sens. Actuators B 73 (2001) 89–94.
[16] X. Song, Q. Qi, T. Zhang, C. Wang, A humidity sensor based on KCl-doped $SnO_2$ nanofibers, Sens. Actuators B 138 (2009) 368–373.
[17] Q. Qi, Y. Feng, T. Zhang, X. Zheng, G. Lu, Influence of crystallographic structure on the humidity sensing properties of KCl-doped $TiO_2$ nanofibers, Sens. Actuators B 139 (2009) 611–617.
[18] Z. Li, H. Zhang, W. Zheng, W. Wang, H. Huang, C. Wang, A.G. MacDiarmid, Y. Wei, Highly sensitive and stable humidity nanosensors based on LiCl doped $TiO_2$ electrospum nanofibers, J. Am. Chem. Soc. 130 (2008) 5036–5037.
[19] Q. Qi, T. Zhang, S. Wang, X. Zheng, Humidity sensing properties of KCl-doped ZnO nanofibers with super-rapid response and recovery, Sens. Actuators B 137 (2009) 649–655.
[20] W. Wang, Z. Li, L. Liu, H. Zhang, W. Zheng, Y. Wang, H. Huang, Z. Wang, C. Wang, Humidity sensor based on LiCl-doped ZnO electrospun nanofibers, Sens. Actuators B 141 (2009) 404–409.
[21] A. Kaniyoor, R. Imran Jafri, T. Arockiadoss, S. Ramaprabhu, Nanostructured Pt decorated graphene and multi walled carbon nanotube based room temperature hydrogen gas sensor, Nanoscale 1 (2009) 382–386.
[22] P.G. Su, J.F. Tsai, Low-humidity sensing properties of carbon nanotubes measured by a quartz crystal microbalance, Sens. Actuators B 135 (2009) 506–511.
[23] H.D. Hill, C.A. Mirkin, The bio-barcode assay for the detection of protein and nucleic acid targets using DDT-induced ligand exchange, Nat. Protoc. 1 (2006) 324–336.
[24] P.G. Su, I.C. Chen, R.J. Wu, Use of poly(2-acrylamido-2-methylpropane sulfonate) modified with tetraethyl orthosilicate as sensing material for measurement of humidity, Anal. Chim. Acta 449 (2001) 103–109.
[25] G. Sauerbrey, The use of quartz oscillators for weighing thin layers and for microweighing, Z. Phys. 155 (1959) 206–222.
[26] X. Sun, T. Okada, Simultaneous determination of the concentration of methanol and relative humidity based on a single nafion(Ag)-coated quartz crystal microbalance, Anal. Chim. Acta 421 (2000) 83–92.
[27] Y. Okahata, M. Kawase, K. Niikura, F. Ohtake, H. Furusawa, Y. Ebara, Kinetic measurements of DNA hybridization on an oligonucleotide-immobilized 27-MHz quartz crystal microbalance, Anal. Chem. 70 (1998) 1288–1296.
[28] J.H. Noggle, Physical Chemistry, Scott, Foresman and Company, 1989, p.408.

[29] D.R. Lide, CRC Handbook of Chemistry and Physics, 78th edition, 1997–1998, p. 5–79.
[30] V. Bondarenka, S. Grebinskij, S. Mickevicius, V. Volkov, Thin films of poly-vanadium-molybdenum acid as starting materials for humidity sensors, Sens. Actuators B 28 (1995) 227–231.
[31] P.G. Su, L.N. Huang, Humidity sensors based on $TiO_2$ nanoparticles/polypyrrole composite thin films, Sens. Actuator B 123 (2007) 501–507.
[32] P.G. Su, W.C. Li, J.Y. Tseng, C.J. Ho, Fully transparent and flexible humidity sensors fabricated by layer-by-layer self-assembly of thin film of poly(2-acrylamido-2-methylpropane sulfonate) and its salt complex, Sens. Actuators B 153 (2011) 29–36.
[33] A. Kassas, J. Bernard, C. Leliévre, A. Besq, Y. Guhel, D. Houivet, B. Boudart, H. Lakiss, T. Hamieh, Ceramic thick film humidity sensor based on $MgTiO_3$ + LiF, Mater. Res. Bull. 48 (2013) 3987–3993.
[34] L.L. Wang, H.Y. Wang, W.C. Wang, K. Li, X.C. Wang, X.J. Li, Capacitive humidity sensing properties of ZnO cauliflowers grown on silicon nanoporous pillar array, Sens. Actuators B 177 (2013) 740–744.
[35] J. Wang, B.K. Xu, S.P. Ruan, S.P. Wang, Preparation and electrical properties of humidity sensing films of $BaTiO_3$/polystrene sulfonic sodium, Mater. Chem. Phys. 78 (2003) 746–750.
[36] G. Casalbore-Miceli, M.J. Yang, N. Camaioni, C.M. Mari, Y. Li, H. Sun, M. Ling, Investigations on the ion transport mechanism in conduction polymer films, Solid State Ionics 131 (2000) 311–321.
[37] J. Wang, Q. Lin, T. Zhang, R. Zhou, B. Xu, Humidity sensor based on composite material of nano-$BaTiO_3$ and polymer RMX, Sens. Actuators B 81 (2002) 248–253.

## Biographies

**Pi-Guey Su** is currently a professor in Department of Chemistry at Chinese Culture University. He received his BS degree from Soochow University in Chemistry in 1993 and PhD degree in chemistry from National Tsing Hua University in 1998. He worked as a researcher in Industrial Technology Research Institute, Taiwan, from 1998 to 2002. He joined as an assistant professor in the General Education Center, Chungchou Institute of Technology from 2003 to 2005. He worked as an assistant professor in Department of Chemistry at Chinese Culture University from 2005 to 2007. He worked as an associate professor in Department of Chemistry at Chinese Culture University from 2007 to 2010. His fields of interests are chemical sensors, gas and humidity sensing materials and humidity standard technology.

**Wei-Hua Liao** received a BS degree in Environmental Engineering from Da Yeh University in 2015. He entered the MS course of Chemistry at Chinese Culture University in 2015. His main areas of interest are humidity-sensing materials.